Engineering Research Journal
journal homepage: https://erj.journals.ekb.eg/

Finite Element Modeling of Reinforced Concrete beam Strengthened by Concrete Overlay

Ehsan Nabil[1,*], Mohamed Yehia[1], Nehal Magdy[1], Alaa Sherif[1]

[1] Civil Engineering Department, Faculty of Engineering Mataria, Helwan University, Cairo, Egypt
*Corresponding author E-mail: ehsannabil2018@gmail.com

Abstract. This study investigates the flexural behavior of reinforced concrete beams strengthened with a concrete overlay under static loading conditions. Numerical simulations were performed using ABAQUS, and the finite element model was validated against experimental data to ensure accuracy. A comprehensive parametric study was conducted, considering variables such as overlay thickness, the area of longitudinal tensile reinforcement, and the compressive strength of concrete. Key performance indicators—including load-deflection behavior, flexural capacity, and ductility ratio—were analyzed. The findings reveal that increasing the thickness of the concrete overlay leads to a reduction in both flexural stiffness and ultimate moment capacity across all types of interface conditions, compared to the un-strengthened control beam. In contrast, enhancing the compressive strength of the overlay resulted in a 7% increase in load-bearing capacity. Although stiffness improved, a noticeable decrease in ductility was observed, with the ductility ratio reaching 5.8. Furthermore, both higher overlay compressive strength and a greater area of longitudinal reinforcement were associated with improved flexural performance.

Keywords: Ductility, Concrete overlay, R.C beam.

1. Introduction

In recent years, the demand for structural strengthening has increased significantly due to factors such as aging infrastructure, damage from natural disasters, material degradation, and the need to accommodate higher structural loads. Traditional strengthening methods for reinforced concrete (RC) beams—such as externally bonded steel plates [1] and fiber-reinforced polymer (FRP) laminates [2]—have been extensively studied. However, these methods present several limitations: steel plates are heavy and difficult to install, prone to shear failure, and susceptible to corrosion. Ultra-High-Performance Concrete (UHPC), also known as Reactive Powder Concrete (RPC), offers a promising alternative due to

DOI: 10.21608/erj.2025.386478.1239
Received 18 May 2025; Received in revised form 21 June 2025; Accepted 13 August 2025
Available online 01 September 2025

its outstanding compressive strength, durability, and long-term performance. UHPC is a composite material characterized by an optimized particle distribution, a low water-to-binder ratio (typically below 0.25), and a high volume of discontinuous internal fibers [3–6]. When applied in the compression zone of over-reinforced RC beams, UHPC has been shown to enhance both flexural capacity and ductility. Numerous studies have confirmed the effectiveness of UHPC for beam strengthening, and it has been increasingly used in infrastructure applications such as bridges and highways [7, 8], roads [9], and tunnels [10]. Yin et al. [11, 12] reinforced RC slabs with UHPC and conducted loading tests, demonstrating fewer diagonal cracks, greater energy absorption, improved post-cracking ductility, and enhanced flexural hardening. They also found that increasing the overlay thickness led to higher ultimate load capacity. Similarly, Farzad [13] conducted an in-depth study on UHPC-strengthened RC beams, reporting improvements in flexural strength, stiffness, and ductility. A finite element model was developed to predict load-deflection behavior and failure cycles, incorporating damage evolution and fracture mechanisms in both conventional concrete and UHPC. Results revealed that UHPC overlays significantly improve the fatigue performance of bridge decks under cyclic loading. Overall, UHPC has proven to be an effective material for strengthening and repairing RC beams by enhancing crack resistance, flexural performance, and service life. Shishegaran et al. [14] investigated the use of ultrasonic pulse velocity and rebound number methods to estimate compressive strength, while Bigdeli et al. [15] applied nonlinear finite element analysis (FEA) to evaluate the behavior of reinforced concrete tunnels sUCjected to internal water pressure. FEA has demonstrated its reliability in simulating RC beam behavior, with several studies confirming strong agreement between simulation results and experimental data. For instance, Shishegaran et al. [16] used FEA to study flexural strength, ductility, and crack patterns of RC members. Zhu et al. [17] modeled UHPC-RC composite slabs in ABAQUS, incorporating a specialized interface model and crack representation based on UHPC-concrete bond strength, achieving good alignment with experimental observations. Yuan et al. [18] introduced an FEA approach for UHPC-NC composites, capturing fracture and softening behaviors, validated through user-defined subroutines (UEL, UMAT) and experimental comparisons.

This study provides two primary contributions:

1. It proposes the use of high-strength concrete overlay on top of RC beams to reduce brittle failure and enhance ductility by leveraging the overlay's superior compressive strength and long-term stability.
2. It employs finite element analysis to simulate and evaluate the mechanical behavior of strengthened RC beams. The proposed technique (Figure 1) is validated against experimental data from the literature [19], focusing on load-deflection response, crack patterns, and failure modes, a widely accepted approach [20, 21].

A parametric study was conducted to investigate the influence of overlay thickness, longitudinal reinforcement area, and concrete strength.

2. Experimental Program

Table 1 outlines the main specifications of the analyzed beams. All beams are reinforced with two 16 mm diameter tensile bars and two 12 mm diameter compression bars, accompanied by 10 mm diameter stirrups placed at 200 mm intervals. While the total beam depth remains constant at 400 mm, the thickness of the concrete overlay varies. Shear connectors, 10 mm in diameter and spaced at 400 mm, are

installed at the interface between the reinforced concrete (RC) and the upper concrete (UC) layers, following the GB50017-2003 [22] standard, which mandates a minimum embedment depth of ten times the connector diameter.

A four-point bending test is applied, with 600 mm between the loading points and a clear span of 1800 mm, as shown in Figure 2. Among the 11 beams, 10 are strengthened with an upper layer, while 1 serves as an un-strengthened control. The studied parameters include: (a) overlay thickness, (b) area of longitudinal tensile reinforcement, and (c) compressive strength of the upper layer. Beam labels follow the format UC30-16-30, where “UC” indicates upper layer reinforcement, 30 mm is the overlay thickness, 16 mm is the diameter of the tensile bar, and 30 MPa is the concrete strength. The control beam is labeled "CB." Finite element models are illustrated in Figures 1 and 2.

3. Finite Element Model.

In this study, ABAQUS is employed to simulate the beams, accurately capturing the nonlinear behavior of the materials. The model assumes perfect bonding, meaning no slip occurs between the reinforcement and concrete or between the upper concrete (UC) layer and the underlying concrete. To avoid stress concentrations, rigid plates are placed at both the support and loading locations. The concrete, UC layer, and plates are modeled using C3D8R solid elements, while the steel reinforcement and shear connectors are represented with T3D2 truss elements.

A binding constraint is applied between the plates and beams, and contact interactions are defined between the steel bars and concrete using internal surface contact. The UC layer is connected to the RC beam using shear connectors, with the traction-separation model used to simulate their interfacial behavior. The beams are simply supported with the following boundary conditions: at the left end, displacements U1, U2, and U3 are fixed (equal to zero), along with rotations UR2 and UR3; at the right end, U1 and U2 displacements and UR2 and UR3 rotations are restrained.

The "Tie" constraint models the interaction between the beam and the plates, while the "Embedment" technique is applied to represent the interaction between the beam, reinforcement, and connectors. The mesh size for the finite element model is set to 20 × 20 mm, as suggested in previous studies [20, 21]. The model configuration is shown in Figure 3.

3.1 Concrete.

In ABAQUS, concrete behavior can be modeled using two main approaches: the Concrete Smeared Cracking model and the Concrete Damaged Plasticity (CDP) model [23]. While the smeared cracking model is typically applied in dynamic load scenarios, the CDP model is more versatile and suitable for both static and dynamic load simulations. Lee et al. [24] used ABAQUS to analyze RC beams, assuming perfect bonding between concrete and reinforcement. Their study showed that the tension damage patterns from the finite element analysis closely matched experimental crack formations, and the model accurately predicted ultimate strength, deformation, and stress responses, aligning well with test results.

The CDP model is also known for its numerical stability and reduced convergence issues, making it a reliable option for concrete simulation. Accurate use of the CDP model requires defining key parameters that describe the concrete’s mechanical behavior. These values are typically sourced from the ABAQUS documentation [25]. Raza et al. [26] demonstrated that using these parameters yields results that strongly correlate with experimental findings, validating their effectiveness. Consequently, the same parameters

are adopted in this study, as listed in Table 2. The corresponding mechanical properties of the simulated concrete are detailed in Table 3.

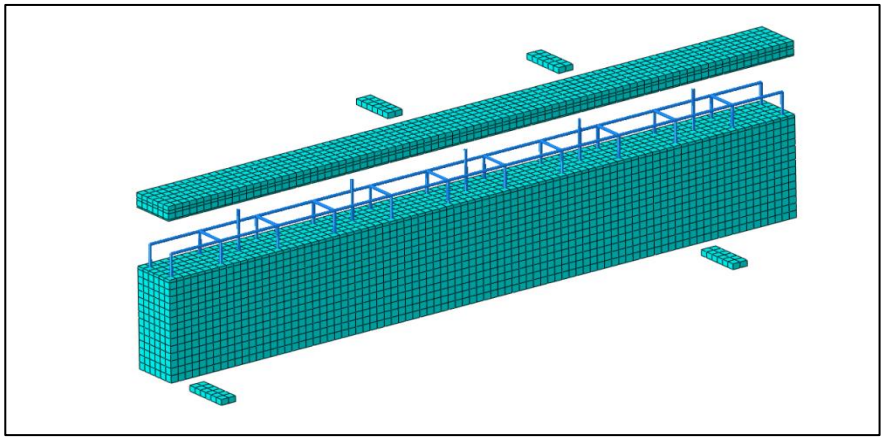

Figure 1: Finite element model of UC layer reinforced beam.

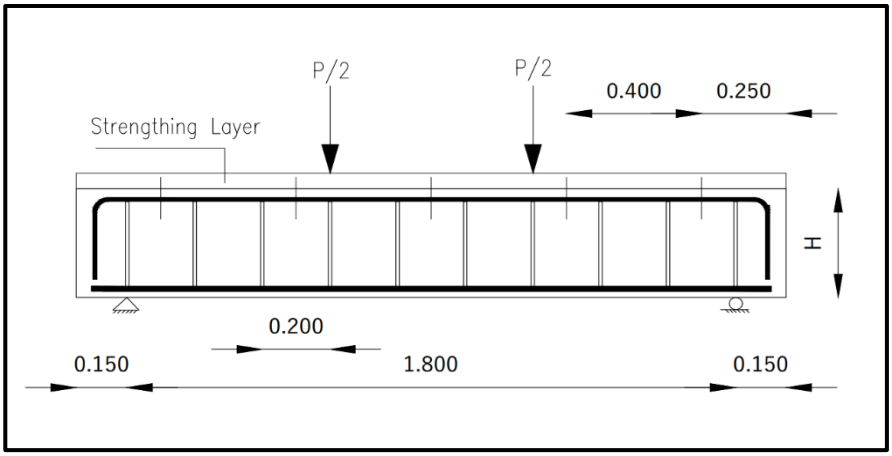

(a)

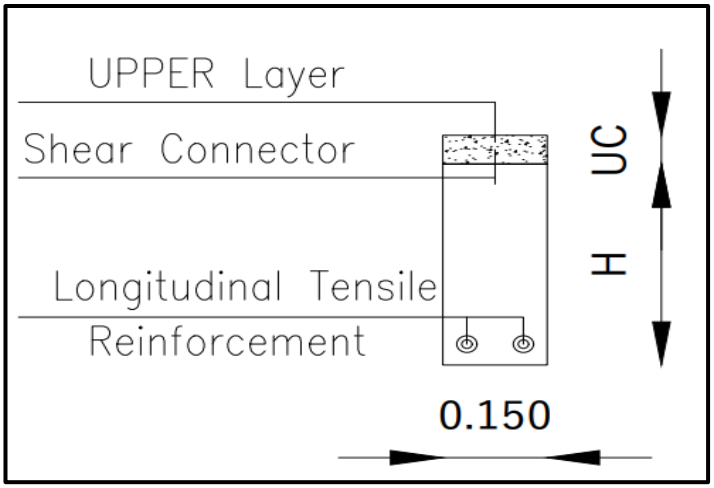

(b)

Figure 2: Theoretical beam size: (a) elevation; (b) sectional view.

Table 1: Parameters of the beams.

Beam	Diameter of longitudinal tension re-bar (mm)	Thickness of upper layer (mm)	Strength of concrete (MPa)	
			Upper layer	Lower layer
CB	16	-	30	30
UC50-12-30	12	50	30	30
UC50-16-30	16	50	30	30
UC50-18-30	18	50	30	30
UC50-20-30	20	50	30	30
UC40-16-30	16	40	30	30
UC60-16-30	16	60	30	30
UC70-16-30	16	70	30	30
UC80-16-30	16	80	30	30
UC50-16-35	16	50	35	30
UC50-16-40	16	50	40	30

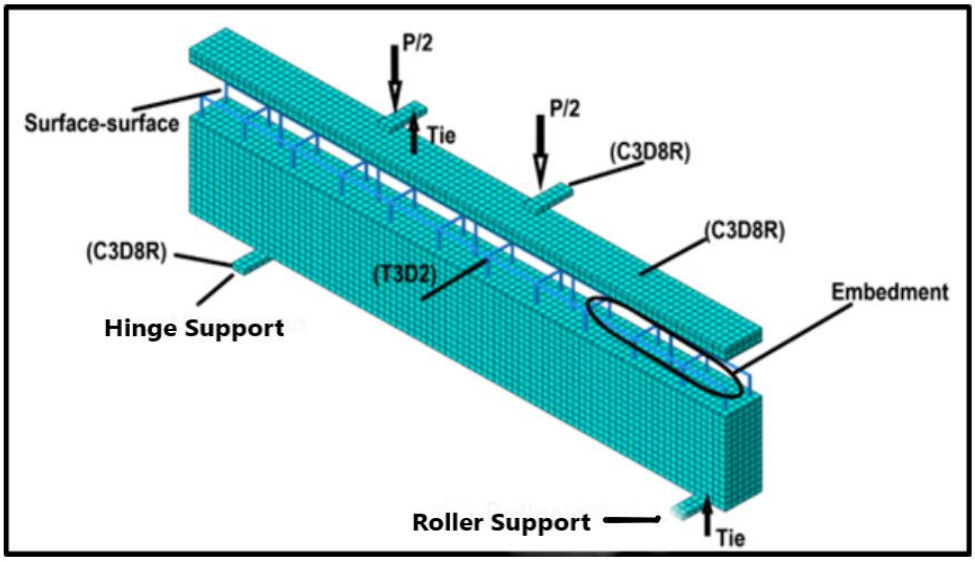

Figure 3: Finite element model.

Table 2: Plastic damage model parameters.

Parameters	Values
Expansion angle	36°
Eccentricity	0.1
fb0/fc0	1.16
K	0.667
Viscosity coefficient	0.01

Table 3: Mechanical properties of concrete.

Item	Fcu (MPa)	Ft (MPa)	Ec	v
Value	30.0	2.27	31553	0.2

The concrete constitutive model in this study is based on the GB 50010-2010 code for concrete structure design [27]. Figure 4 illustrates the constitutive relation curve, along with the compression and tension damage parameters, which are crucial for accurately simulating the material's mechanical behavior.

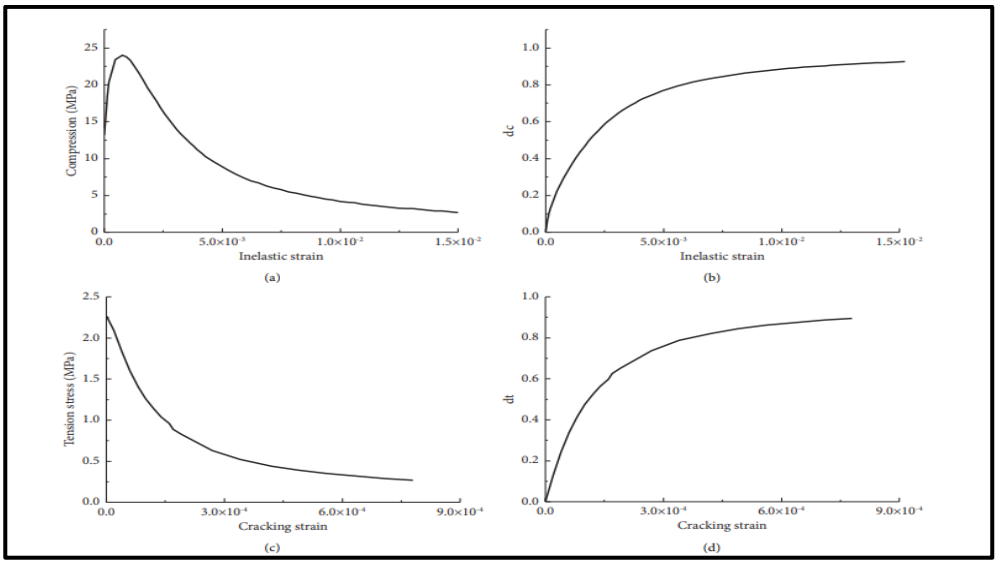

Figure 4: Constitutive relation curve of concrete: (a) compressive stress vs. inelastic strain; (b) compressive damage vs. inelastic strain; (c) tension stress vs. cracking strain; (d) tension damage vs. cracking strain.

3.2 Rebar.

In this study, the longitudinal reinforcement and stirrups are modeled using an elastoplastic approach. The rebar's linear elastic behavior is defined by its elastic modulus and Poisson's ratio, while its plastic behavior is characterized by yield stress and plastic strain properties. The specific mechanical properties of the rebar are listed in Table 4.

3.3 Upper layer.

To determine the constitutive relationship for the upper layer, Zhang et al. [28] performed axial tension tests on upper-layer specimens. Their study analyzed the axial tension parameters of four different fiber-reinforced layers using a control variable method. Building on these results, Prem et al. [29] reviewed various formulations of the upper layer's stress-strain curve. They examined the impact of different steel fiber contents on the upper layer’s mechanical performance, evaluating its stress-strain characteristics. Based on experimental data, they developed a compressive constitutive model that accurately represents the upper layer's stress-strain behavior, showing strong agreement with experimental findings. The tensile

stress-strain relationship for the upper layer used in this study is expressed by the following formulas:

$$\sigma_{(\varepsilon)} = \frac{f_{ct}\varepsilon}{\varepsilon_{ca}} \quad 0 \le \varepsilon \le \varepsilon_{ca}, \qquad (1)$$

$$\sigma_{(\varepsilon)} = f_{ct} \quad \varepsilon_{ca} \le \varepsilon \le \varepsilon_{pc}, \qquad (2)$$

Describing the tensile stress-strain relationship for the upper layer, where:

- σ(ε) = Tensile stress of the upper layer
- ε = Tensile strain
- fct = Elastic ultimate tensile strength
- εca = Elastic ultimate tensile strain
- εpc = Ultimate tensile strain

The tensile stress-strain formula is generally represented as a piecewise function, reflecting the material's behavior in various strain regions (elastic, strain-hardening, softening, or failure).

$$y = \begin{cases} Ax + (6 - 5A)x^5 + (4A - 5)x^6, & (0 \le x \le 1), \\ \dfrac{x}{\alpha(x-1)^2 + x}, & (x \ge 1), \end{cases} \qquad (3)$$

Table 4: Mechanical properties of rebar.

Rebar	Diameter (mm)	Elasticity modulus (GPa)	Poisson's ratio	Yield strength (MPa)
Stirrup	10	200	0.3	500
Compression rebar	12	200	0.3	500
Tension rebar	16	200	0.3	500

3.4 Contact Interface Between Upper Layer and Concrete

The contact interface between the upper concrete (UC) layer and the concrete beam is crucial for determining the shear resistance and bond strength of the composite structure. Two main approaches are used to define the shear resistance at this interface:

1. AASHTO [30] Approach: Provides guidelines for the minimum shear resistance at the interface.
2. ACI [31] Approach: Assumes pre-existing cracks at the interface, considering only the friction coefficient and shear-friction reinforcement in shear strength calculations, and uses a conservative method that disregards bond strength between concrete layers poured at different times.

Interface Simulation in ABAQUS [32-33]:
ABAQUS offers two traction-separation models to accurately simulate the interface behavior:

- Cohesive elements with a specific thickness to simulate adhesive bonding.
- Surface-to-surface contact properties for a direct interface simulation.

Method Used in This Study:
Since no adhesive is applied between the UC layer and the lower concrete, the adhesive thickness is considered zero. Instead, connectors serve as the primary connecting elements. The traction-separation model in ABAQUS is used to simulate the interface behavior between the upper layer and the RC beam. The slip parameters for the contact surface between the connectors, upper layer, and concrete are listed in Table 5.

Table 5: Slip parameters of upper layer and concrete interface

Parameters	Values
K_{nn} (N/mm3)	1358
Ks, Kt (N/mm3)	20358
t_n, t_s, t_t (MPa)	5.63
Total/plastic deflection	0.241
Viscosity coefficient	0.01
Friction coefficient	0.70

4 Calculation Method of Yield Load

To determine the yield load on the load-deflection curve, this study uses the "farthest point method" introduced by Feng et al. [34]. This method identifies the yield point as the point that is farthest from the straight line drawn between the origin and the peak point on the load-deflection curve.
The steps for identifying the yield load, as shown in Figure 5, are:

1. Draw a straight line from the origin to the peak point on the load-deflection curve.
2. Identify the point that is farthest from this line—this represents the yield point.
3. If there are multiple such points, the average of these points is taken as the final yield point.
4. Draw a line parallel to the original straight line that is tangent to the load-deflection curve.

The tangent point on the curve represents the yield point, and the corresponding load value is the yield load.

5 Ductility Analysis

Deflection ductility is an important mechanical performance parameter, especially when assessing the flexural behavior of reinforced concrete (RC) beams both before and after strengthening. The ductility coefficient (μ) is determined using the following formula:

$$\mu = \Delta u / \Delta y, \quad (4)$$

where:

- μ = Deflection ductility coefficient
- Δ = Deformation parameter (e.g., deflection, strain, section curvature, rotation angle)
- Δu = Ultimate deflection
- Δy = Initial yield deflection

This ductility coefficient helps assess the energy absorption and post-yield behavior of the beam, which is essential for structural safety and performance evaluation.

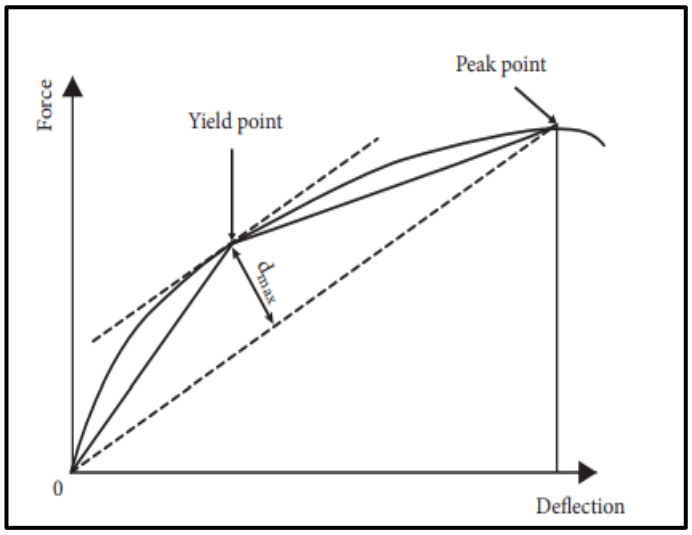

Figure 5: Schematic diagram of farthest point method

6 Results and Discussion

6.1 Verification of the Finite Element Model

The accuracy of the finite element model (FEM) developed in ABAQUS was confirmed by verifying its results with experimental data, specifically examining the load-deflection curve, crack patterns, and failure mode. The FEM of the control beam (CB) was compared with experimental outcomes, verifying the model's accuracy based on the load-deflection curve, crack distribution, and failure mode.

6.2.1 Load-Deflection Curve:

The finite element model (FEM) developed in ABAQUS successfully simulated the entire loading process of the control beam (CB). The verifying of the FEM results with experimental data, shown in Figure 6, indicates that the FEM closely replicates the experimental load-deflection curve. The cracking load predicted by the FEM is 100 kN, slightly higher than the experimental 90 kN, while the yield load is 242.5 kN in the FEM, compared to 198 kN in the experiment. The peak load predicted by the FEM is 255.828 kN, which is reasonably close to the experimental 243 kN, confirming the accuracy of the model.
Despite the close agreement, minor deviations exist between the FEM and experimental results. These deviations are attributed to real-world factors such as concrete shrinkage and hydration effects, which reduce stiffness in the experimental setup but are not explicitly modeled in the FEM. Additionally, boundary conditions in the actual experiment may not be perfectly rigid, which can lead to reduced stiffness in the experimental results. The FEM also assumes a perfect bond between the rebar and concrete, whereas bond slip in the experimental setup could cause slightly lower stiffness and peak load. Overall, the FEM's performance closely matches the experimental data, with these minor differences stemming from material behaviors and boundary conditions difficult to replicate exactly in simulations.

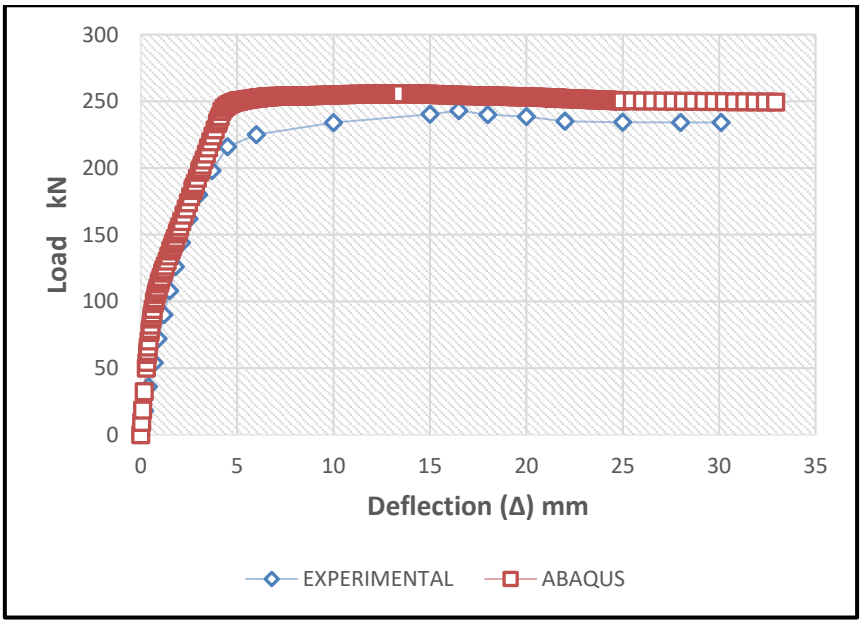

Figure 6: Verifying between the ABAQUS result and experimental reading for Mid-span longitudinal steel bar strain for strengthen beam CB.

6.2.2 Failure Mode

The results confirm that the finite element model accurately replicates the crack patterns and failure behavior of the experimental beams, reinforcing its validity and reliability for structural analysis.

The finite element model (FEM) accurately replicates the failure pattern and crack distribution observed in the reinforced concrete (RC) beams. Experimentally, the primary failure mechanism involves the crushing of the upper concrete layer, primarily resulting from the high tensile reinforcement at the bottom. In the simulation, ABAQUS's DAMAGET output effectively captures and visualizes the damage zones, offering valuable insight into the structural failure process.

As shown in Figure 7, the comparison between FEM and experimental results reveals a high degree of agreement in failure modes and crack development. Both approaches show that initial vertical cracks emerge at the bottom center of the beam during the early stages of loading. As the load increases, these cracks expand in length and width. Eventually, at the peak load, the top concrete crushes due to excessive compressive stress, and the bottom longitudinal reinforcement yields, indicating ductile behavior. This strong correlation confirms the FEM's capability to reliably simulate the structural response and failure characteristics of the RC beams.

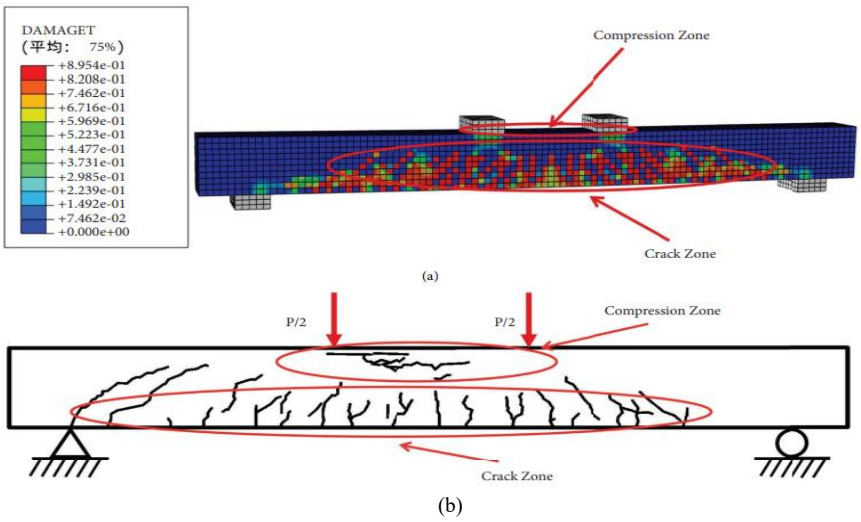

Figure 7: Crack distribution: (a) CB (FEM); (b) CB(EXP).

6.2 Parameter Study.

To evaluate how different factors affect RC beams strengthened with an upper concrete layer, a parametric study was conducted using specimen UC50-16-30 as the reference. The analysis focused on three key variables: the thickness of the upper layer, the cross-sectional area of the longitudinal tensile reinforcement, and the compressive strength of the upper layer concrete. Their effects were assessed by examining the load–deflection behavior, flexural capacity, and ductility of the beams. Figure 8, 9 and 10 presents the load–deflection curves for beams with varying parameters, illustrating the influence of each factor on structural performance.

6.2.1 Thickness of UHPC Layer.

This study aims to assess the impact of varying the thickness of the upper concrete layer on the flexural behavior of reinforced concrete (RC) beams strengthened with a top overlay. The thickness was incrementally increased from 40 mm to 80 mm in 10 mm steps. Finite element analysis (FEA) results presented in Figures 8(a) to 8(d) reveal that all beams exhibited similar initial stiffness before cracking, indicating that upper layer thickness has minimal effect during the elastic stage. However, after the formation of the first crack, a noticeable drop in flexural stiffness was observed as the upper layer became thicker. This reduction was accompanied by increased vertical and horizontal deflections, indicating reduced structural rigidity and weaker composite interaction.

Table 6 shows that the peak load decreased from 245.1 kN to 231.4 kN with increasing upper layer thickness, representing reductions of 2.62%, 3.3%, 4.5%, and 6%, respectively. Moreover, the deflection ductility coefficient decreased almost linearly from 6.4 to 5.3, confirming that thicker upper layers reduce the ductile capacity of the beams. The results suggest that thicker overlays hinder stress transfer efficiency and weaken the composite action between the upper and lower concrete layers. In contrast, thinner layers (40–60 mm) maintain better interaction, resulting in improved stiffness, higher load capacity, and more uniform stress distribution across the section.

In conclusion, overlays with thicknesses between 40 mm and 60 mm were found to be the most effective. They offered minimal reduction in peak load, which indicates strong composite behavior and efficient

shear transfer through the connectors, allowing the beam to behave more like a monolithic unit. When the thickness exceeded 60 mm, the connectors became less effective in resisting increased shear forces, leading to lower stiffness, greater deflections, and reduced ductility. These findings highlight the importance of optimizing the top layer thickness to achieve superior structural performance and maximize the effectiveness of the composite action in RC beams. Figure 9 visually confirms these patterns, showing consistent failure modes across the specimens.

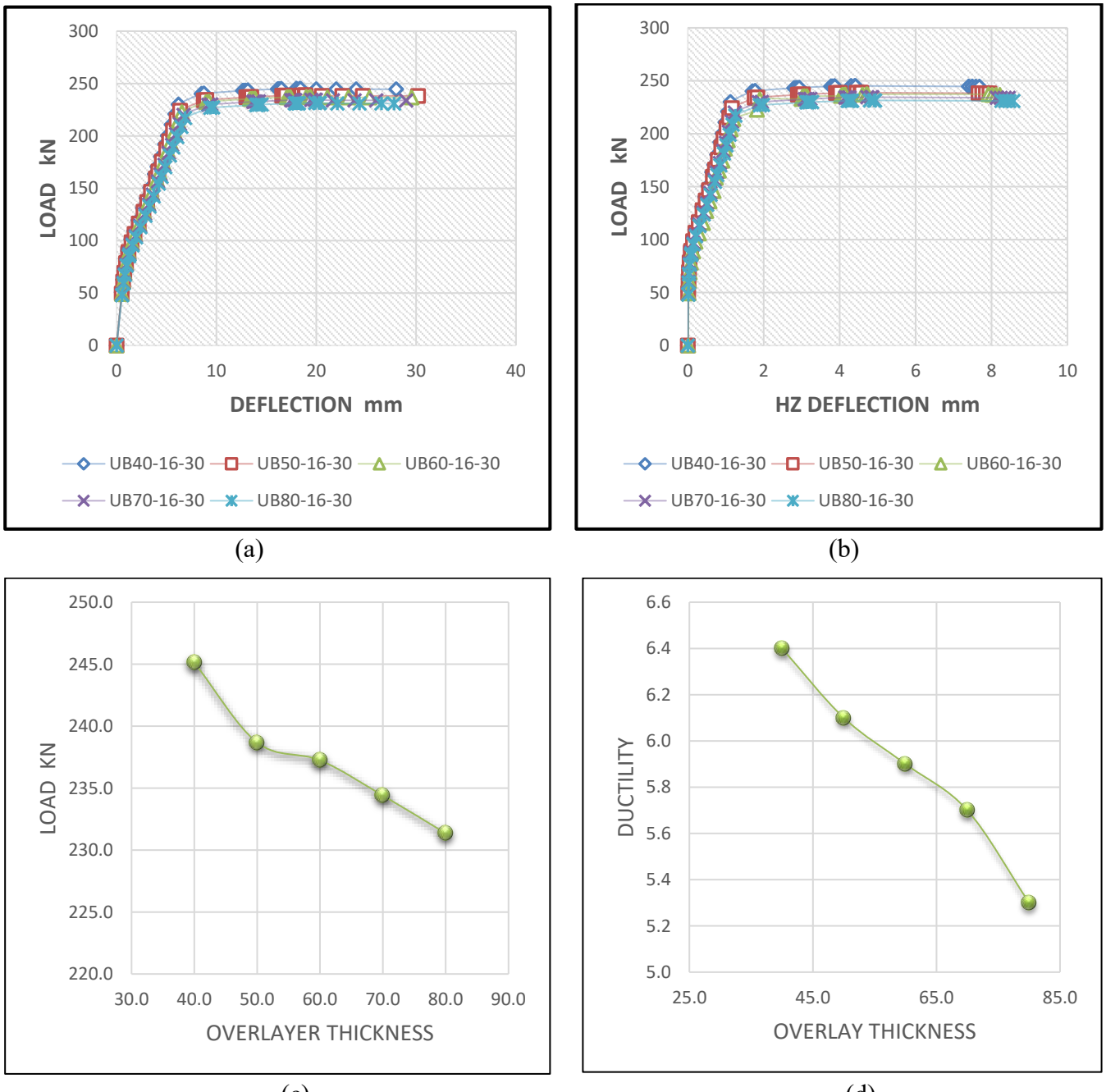

Figure 8: illustrates the effect of varying upper layer thickness on the peak load of reinforced concrete beams. (a) shows the relationship between vertical deflection and applied load, (b) presents the horizontal slip versus load, (c) demonstrates how the peak load changes with different top layer, and (d) demonstrates how the ductility ratio changes with different top layer.

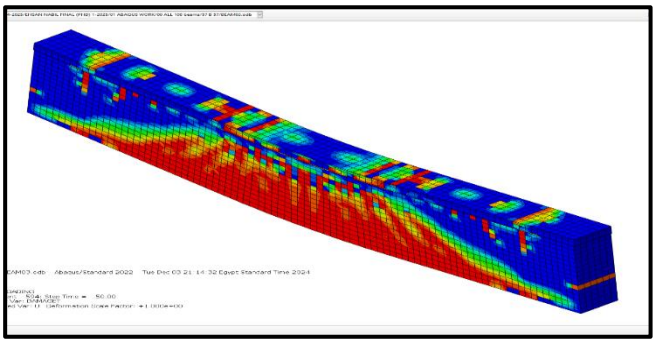

(a) 40 mm

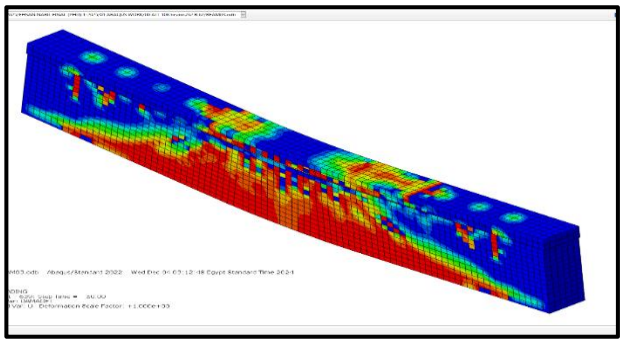

(b) 50 mm

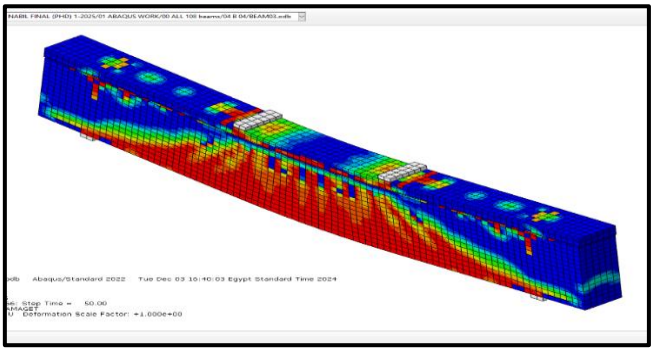

(c) 60 mm

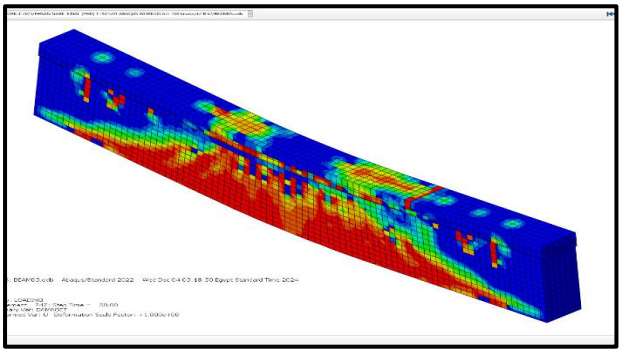

(d) 70 mm

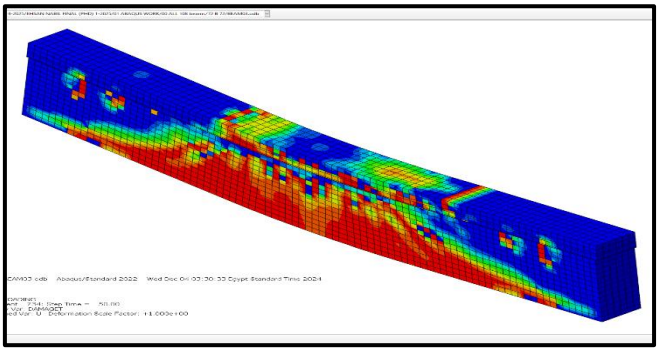

(e) 80 mm

Figure 9: Modes of failure for layers thickness of upper layer for all beams

Table 6: Comparison of peak load, stiffness, vertical, horizontal deflection and ductility coefficient for overlay thickness**.**

Beam	Pmax (KN)	$\Delta_{VL.}$ (mm)	Stiffness (KN/mm)	$\Delta_{HZ.}$ (mm)	μ
UC40-16-30	245.1	18.0	13.6	4.3	6.4
UC50-16-30	238.68	18.5	12.9	4.45	6.1
UC60-16-30	237.2	19.0	12.5	4.6	5.9
UC70-16-30	234.4	19.5	12.0	4.7	5.7
UC80-16-30	231.4	19.9	11.6	4.8	5.3

6.2.2 Areas of tension Rebar.

Based on the reference beam UC50-16-30, the influence of varying the diameter of longitudinal tensile reinforcement on the flexural behavior of reinforced composite beams was thoroughly investigated. Finite element analysis (FEA) results for different reinforcement configurations—2Φ12, 2Φ16, 2Φ18, and 2Φ20—are depicted in Figures 10(a) through 10(d). The load-deflection curves demonstrate a clear and consistent pattern: increasing the area of tensile reinforcement significantly enhances both the ultimate flexural capacity and stiffness of the beams. However, this improvement in strength is generally offset by a reduction in ductility. For example, when the reinforcement is reduced to 2Φ12 (as in UC50-12-30), the peak load decreases by 30% to 167 kN, while the ductility coefficient increases slightly by about 1.05%. In contrast, increasing the reinforcement area to 2Φ18 and 2Φ20 results in substantial strength gains, raising the peak loads to 352.66 kN and 424.53 kN—an increase of 32.32% and 43.78%, respectively, as listed in Table 7.

Regarding deformation, vertical deflection diminishes with larger reinforcement due to the resulting increase in beam stiffness. Meanwhile, horizontal slip at the interface remains minimal under normal service loads, provided the shear connectors have adequate capacity. Under ultimate loads, however, slip may increase slightly. Energy absorption capacity—dependent on both strength and ductility—initially improves as reinforcement increases, but further reinforcement (e.g., 2Φ20) leads to reduced ductility, limiting the beam's ability to dissipate energy. This may shift the failure mode toward a more brittle, compression-dominated behavior, which must be considered during design to avoid premature failure. Ultimately, optimizing the reinforcement area requires a careful balance: while larger reinforcement enhances strength and stiffness, it may adversely affect ductility and reduce the beam's capacity to accommodate large deformations, potentially compromising overall structural resilience. Figure 11 visually confirms these patterns, showing consistent failure modes across the specimens.

Table 7: Comparison of peak load, stiffness, vertical, horizontal deflection and ductility coefficient for tension Rebar.

Beam	Pmax (KN)	$\Delta_{VL.}$ (mm)	Stiffness (KN/mm)	$\Delta_{HZ.}$ (mm)	μ
UC50-12-30	167	19	8.7	4.47	6.4
UC50-16-30	238.68	18.5	12.9	4.45	6.1
UC50-18-30	352.66	18	19.6	4.4	5.9
UC50-20-30	424.53	17.3	24.54	4.25	5.7

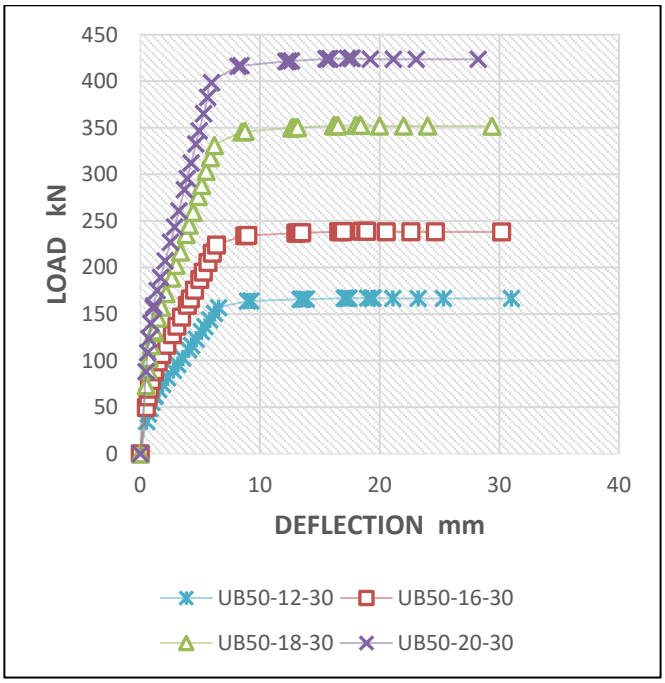

(a)

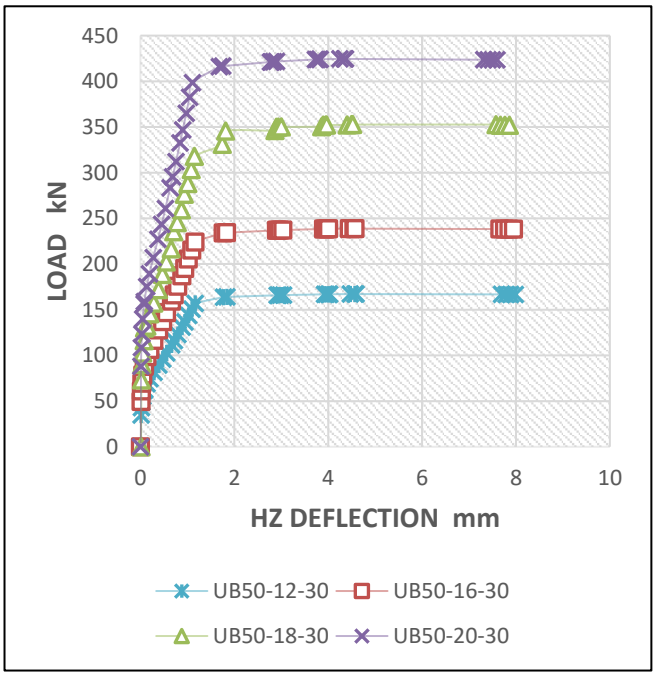

(b)

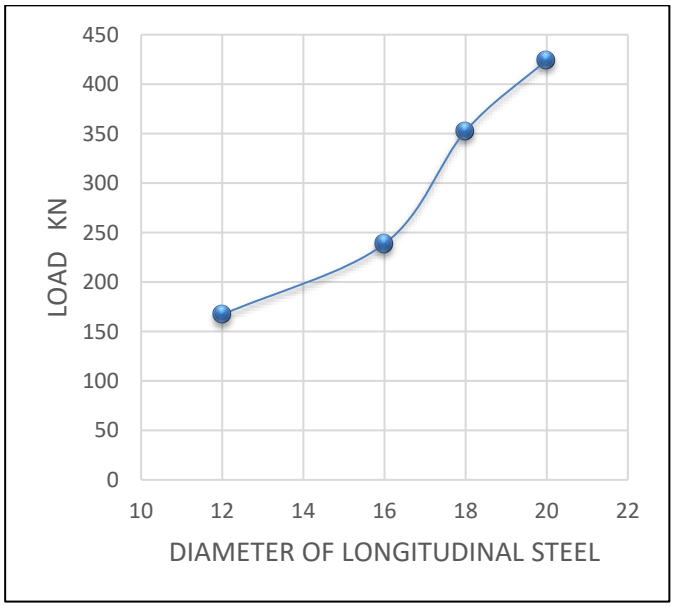

(c)

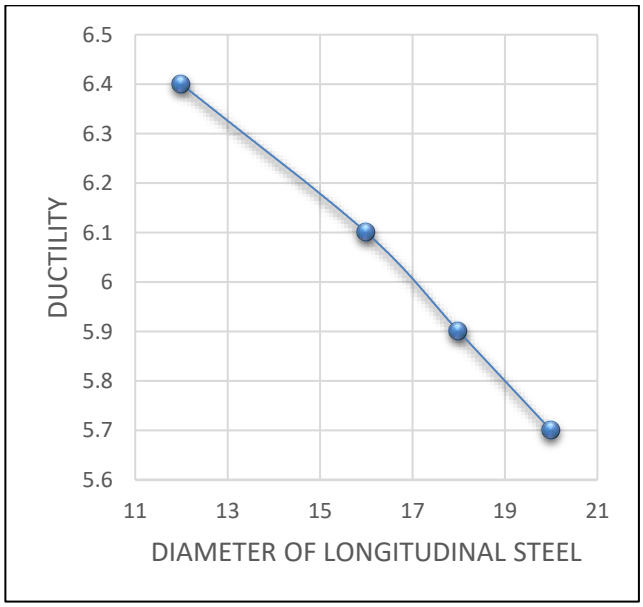

(d)

Figure 10: illustrates the effect of varying area of tension rebar on the peak load of reinforced concrete beams. (a) shows the relationship between vertical deflection and applied load, (b) presents the horizontal slip versus load, (c) demonstrates how the peak load changes with different area bar, and (d) demonstrates how the ductility ratio changes with different area bar.

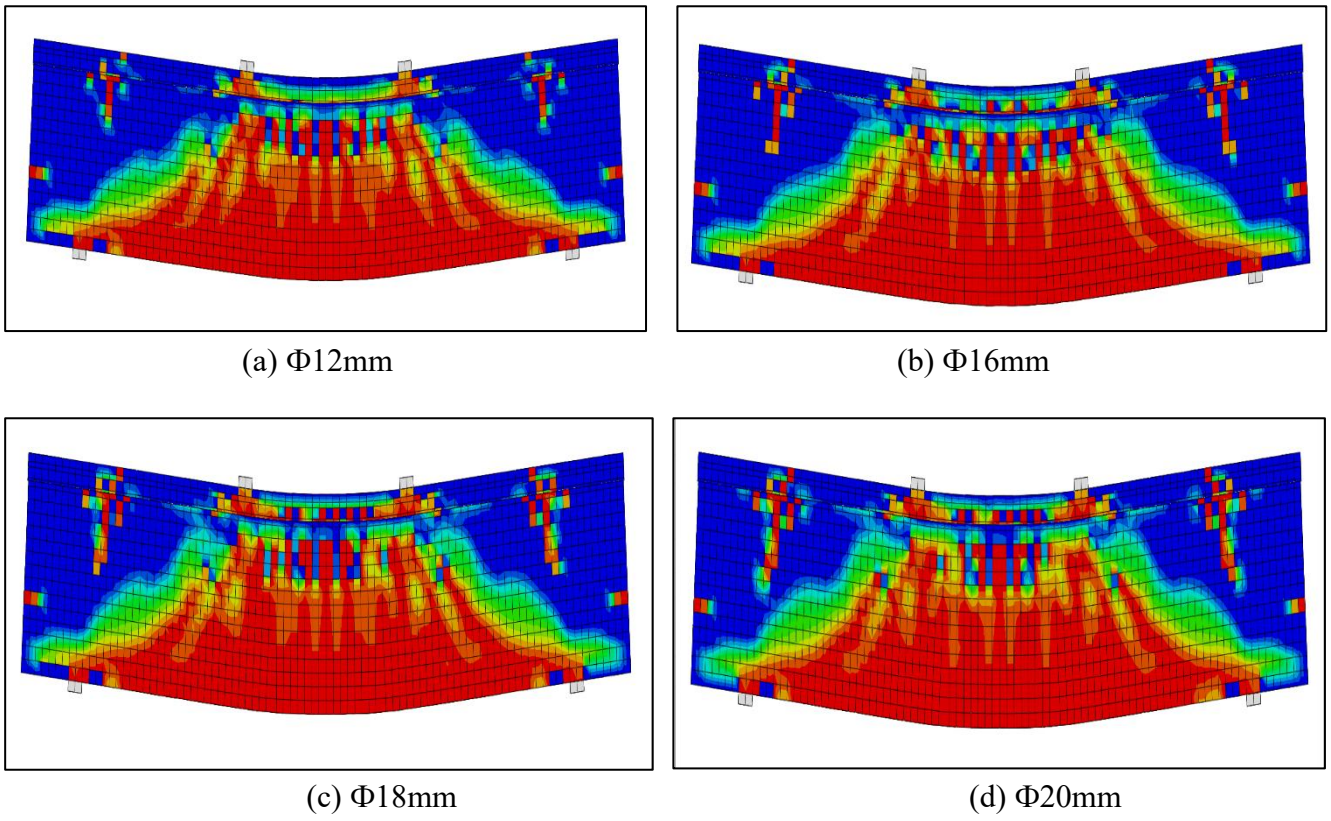

(a) Φ12mm (b) Φ16mm

(c) Φ18mm (d) Φ20mm

Figure 11: Modes of failure for area of tension rebar for all beams.

6.2.3 Concrete Strength.

Building upon the benchmark specimen UC50-16-30, the influence of upper concrete layer compressive strength on the flexural behavior and ductility of composite beams was systematically examined. In this investigation, the compressive strength of the upper concrete layer was increased incrementally by 5 MPa to produce two additional specimens: UC50-16-35 and UC50-16-40, with strengths of 35 MPa and 40 MPa, respectively. The corresponding load-deflection responses, obtained through finite element simulations, are illustrated in Figures 12(a), through 12(d).

While theoretical flexural models predict that increasing concrete compressive strength could enhance the flexural capacity of RC beams by 15–20%, the actual improvement observed in this study was comparatively limited. Specifically, the peak load increased by only 4% for UC50-16-35 and 8% for UC50-16-40 relative to UC50-16-30. This modest increase can be attributed to the premature yielding of the shear connectors, which restricts the full engagement of the concrete's compressive strength. In other words, once the shear connectors reach their load-carrying capacity, further increases in concrete strength do not translate effectively into improved structural performance.

Additionally, the deflection ductility coefficients decreased with rising concrete strength, from 6.4 in UC50-16-30 to 5.9 in UC50-16-35 and 5.8 in UC50-16-40. This reduction in ductility is likely due to the stiffer response of higher-strength concrete, which reduces the beam's ability to deform plastically before failure. The increase in interface slips at ultimate load—approximately 10% higher in UC50-16-40 compared to UC50-16-30—also indicates a reduction in composite action. These trends suggest that the connectors in higher-strength specimens reach their capacity earlier, leading to a shift in the failure mecha-

nism. For instance, in UC50-16-30, failure begins with concrete crushing in the compression zone, followed by gradual yielding of the shear connectors. In contrast, UC50-16-40 shows initial failure through connector yielding, which limits the concrete's ability to reach its ultimate strain.

These findings, summarized in Table 8, clearly illustrate the trade-offs between strength, ductility, and interface behavior. While increasing the upper layer concrete strength does result in modest gains in peak load and stiffness, these benefits are constrained by the unchanged connector capacity. As a result, further improvements in performance cannot be realized without simultaneously enhancing the shear transfer system. This underscores the importance of holistic structural design: improvements in material properties must be matched by corresponding adjustments in connection detailing to achieve optimal and balanced performance in composite RC beam systems. Figure 13 illustrates the failure modes of beams with varying compressive strengths.

Table 8: Comparison of peak load, stiffness, vertical, horizontal deflection and ductility coefficient for overlay Concrete Strength.

Beam	Pmax (KN)	$\Delta_{VL.}$ (mm)	Stiffness (KN/mm)	$\Delta_{HZ.}$ (mm)	μ
UC50-16-30	238.68	18.5	12.9	4.45	6.1
UC50-16-35	248.2	17.8	14.0	4.7	5.9
UC50-16-40	257.7	17.4	14.8	4.9	5.8

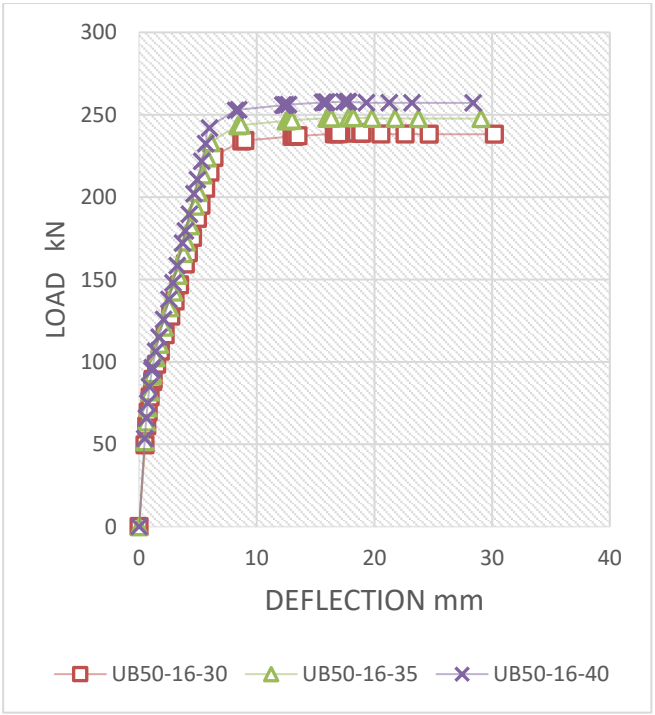

(a)

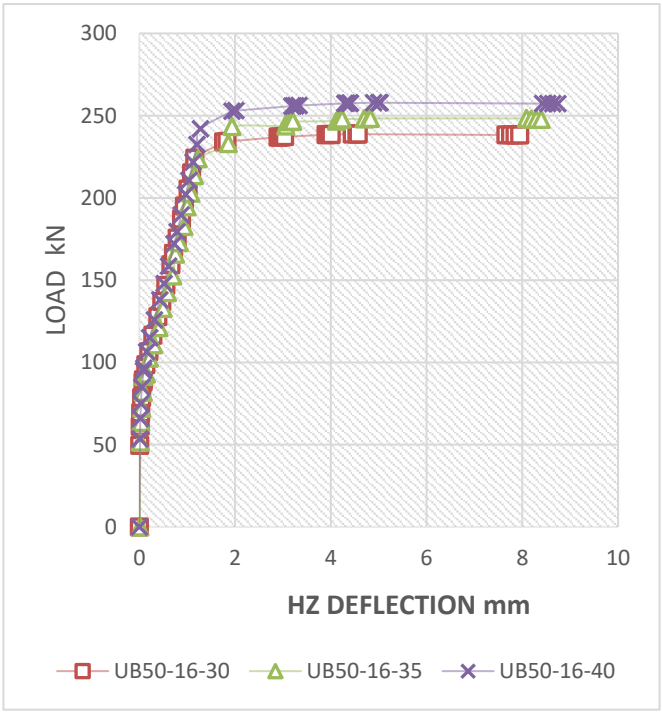

(b)

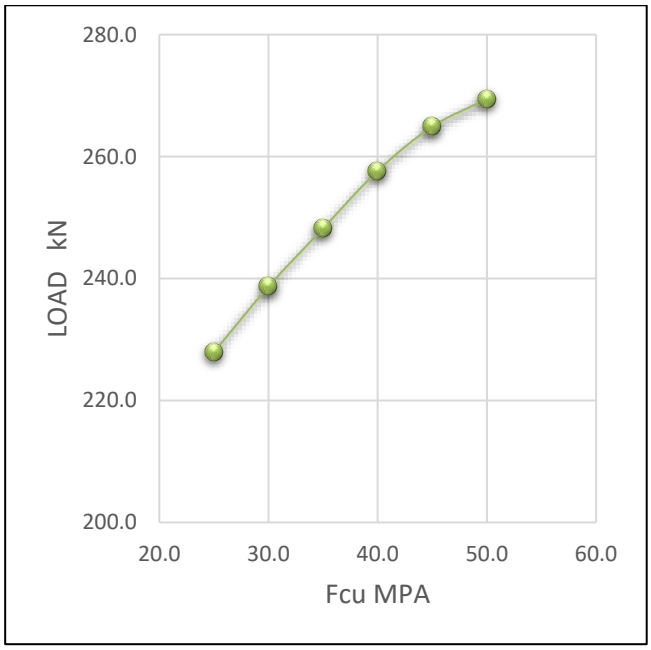

(c)

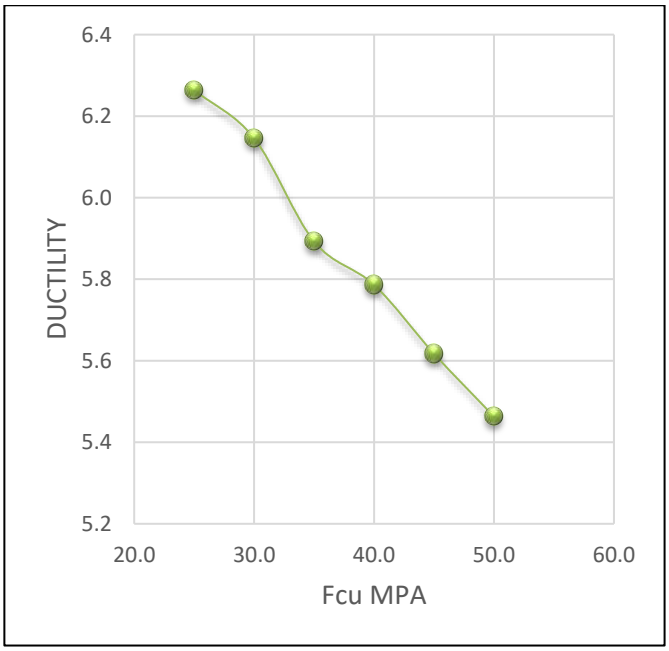

(d)

Figure 12: illustrates the effect of varying concrete strength on the peak load of reinforced concrete beams. (a) shows the relationship between vertical deflection and applied load, (b) presents the horizontal slip versus load, (c) demonstrates how the peak load changes with different concrete strength, and (d) demonstrates how the ductility ratio changes with different concrete strength.

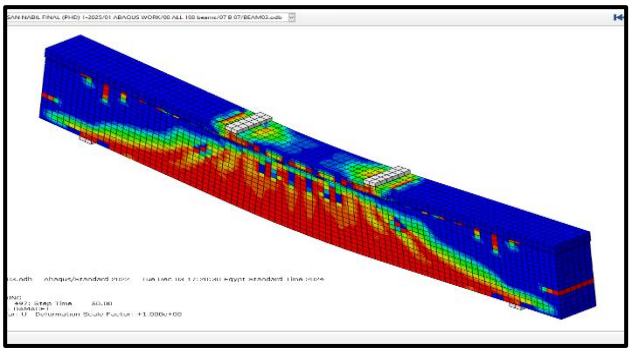

FCU 30

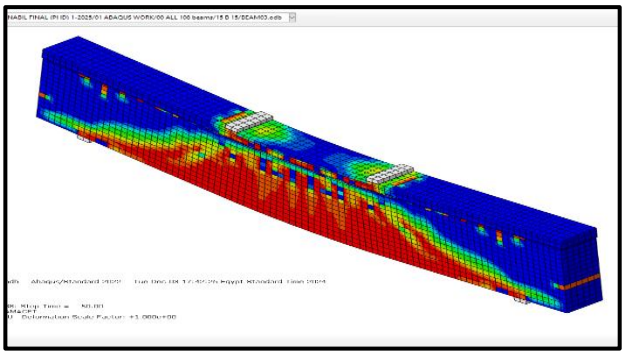

FCU 35

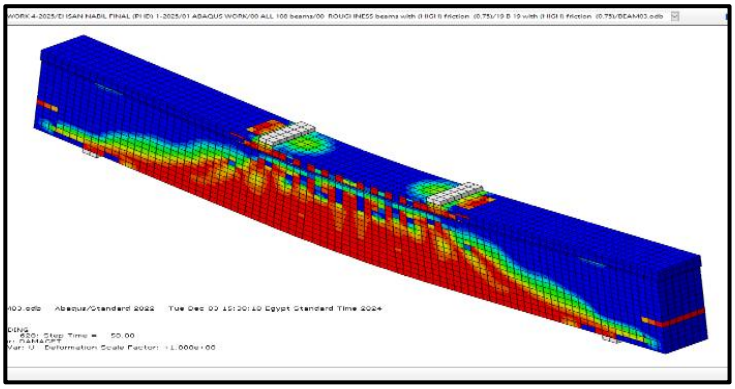

FCU 40

Figure 13: Crack pattern for different compressive strength

Conclusions

This study comprehensively investigated the flexural performance of composite concrete beams by varying key structural parameters: the thickness of the upper concrete layer, the area of longitudinal tension reinforcement, and the compressive strength of the top concrete layer. The primary objective was to assess how each parameter influences the beams' strength, stiffness, ductility, and overall structural efficiency.

1. The finite element model (FEM) accurately simulated the complete loading process of the reference beam (CB). Its predictions for the load-deflection response, flexural capacity, and failure mode aligned closely with the experimental results, confirming the model's validity and reliability.

2. The optimal performance was observed in beams with upper layer thicknesses ranging from 40 mm to 60 mm. Within this range, the beams demonstrated the best balance between load-bearing capacity, flexural stiffness, and ductility. Increasing the top layer thickness beyond 60 mm led to a decline in composite action, increased interface slip, and greater vertical and horizontal deflections.

3. Increasing the area of longitudinal tension reinforcement resulted in significant improvements in flexural capacity and stiffness. However, these gains came at the expense of reduced ductility and increased susceptibility to brittle failure, particularly in heavily reinforced specimens.

4. Enhancing the compressive strength of the upper concrete layer from 30 MPa to 40 MPa yielded only modest improvements in load capacity and stiffness. This limited gain is primarily due to the finite capacity of the shear connectors, which restrict the extent to which the additional strength of the concrete can be utilized.

In conclusion, achieving optimal structural performance in composite RC beams requires a well-balanced design strategy. The interplay between upper layer thickness, reinforcement detailing, and concrete strength must be carefully considered in conjunction with sufficient shear connector capacity. Only through such integrated optimization can designers ensure both structural efficiency and safety under flexural loading conditions.

References

[1] S. Altin, O. Anil, and M. E. Kara, "Improving shear capacity of existing RC beams using external bonding of steel plates," Engineering Structures, vol. 27, no. 5, pp. 781–791, 2005.
[2] H. Rahimi and A. Hutchinson, "Concrete beams strengthened with externally bonded FRP plates," Journal of Composites for Construction, vol. 5, no. 1, pp. 44–56, 2001.
[3] N. M. Azmee and N. Shafq, "Ultra-high-performance concrete: from fundamental to applications," Case Studies in Construction Materials, vol. 9, Article ID e00197, 2018.
[4] B. Graybeal, Ultra-High-Performance Concrete, Federal Highway Administration, McLean, VA, 2011.
[5] B. Graybeal, Material Property Characterization of Ultra-High-Performance Concrete, Federal Highway Administration, McLean, VA, 2006.
[6] P. R. Prem, A. Ramachandra Murthy, G. Ramesh, B. H. Bharatkumar, and N. R. Iyer, "Flexural behavior of damaged RC beams strengthened with ultra high-performance concrete," Advances in Structural

Engineering, vol. 89, pp. 2057–2069, 2015. [8] B. Graybeal, UHPC in the U.S. Highway Infrastructure, Federal Highway Administration, McLean, VA, 2009.
[7] B. Graybeal, UHPC in the U.S. Highway Infrastructure, Federal Highway Administration, McLean, VA, 2009.
[8] M. Zhou, W. Lu, J. W. Song, and G. C. Lee, "Application of ultra-high-performance concrete in bridge engineering," Construction and Building Materials, vol. 186, pp. 1256–1267, 2018.
[9] K. H. Khayat and M. Valipour, Design of Ultra High-Performance Concrete as an Overlay in Pavements and Bridge Decks, Missouri University of Science and Technology, Center for Transportation Infrastructure and Safety, Missouri, 2014.
[10] R. Bugers, J. Walraven, G. A. Plizzari, and G. Tiberti, Structural behavior of SFRC tunnel segments during TBM operations, pp. 1461–1467, World Tunnel Congress ITAAITES 2007, Prague, Czech RepUClic, 2007.
[11] H. Yin, W. Teo, and K. Shirai, "Experimental investigation on the behaviour of reinforced concrete slabs strengthened with ultra-high-performance concrete," Construction and Building Materials, vol. 155, pp. 463–474, 2017.
[12] C. Oesterlee, Structural Response of Reinforced UHPFRC and RC Composite Members", Doctoral thesis of Swiss federal Institute of Technology in Lausanne, Lausanne, 2010.
[13] M. Farzad, Retroftting of Bridge Elements SUCjected to Predominantly Axial Load Using UHPC Shell", Doctoral thesis of Florida International University, Miami, 2019.
[14] A. Shishegaran, H. Varaee, T. Rabczuk, and G. Shishegaran, "High correlated variables creator machine: prediction of the compressive strength of concrete," Computers & Structures, vol. 247, no. 247, Article ID 106479, 2021.
[15] A. Bigdeli, A. Shishegaran, M. A. Naghsh, B. Karami, A. Shishegaran, and G. Alizadeh, "Surrogate models for the prediction of damage in reinforced concrete tunnels under internal water pressure," Journal of Zhejiang University - Science, vol. 22, no. 8, pp. 632–656, 2021.
[16] A. Shishegaran, M. R. Ghasemi, and H. Varaee, "Performance of a novel bent-up bars system not interacting with concrete," Frontiers of Structural and Civil Engineering, vol. 13, no. 6, pp. 1301–1315, 2019.
[17] Y. P. Zhu, Y. Zhang, H. H. Hussein, and G. D. Chen, "Numerical modeling for damaged reinforced concrete slab strengthened by ultra-high-performance concrete (UHPC) layer," Engineering Structures, vol. 209, Article ID 110031, 2020.
[18] S. Q. Yuan, Z. Liu, and T. Tong, "Investigation of over nonlocal damage and interface cohesive models for simulating structural behaviors of composite UHPC-NC members," Structures, vol. 28, pp. 2617–2632, 2020.
[19] M. K. Deng, M. Zhang, F. D. Ma, F. Y. Li, and H. Z. Sun, "Flexural strengthening of over-reinforced concrete beams with highly ductile fiber-reinforced concrete layer," Engineering Structures, vol. 231, Article ID 111725, 2021.
[20] L. Liu and S. Wan, "Flexural bearing capacity of reinforced concrete beams reinforced with carbon fiber reinforced plastics strips and ultra-high performance concrete layers," International Journal of Building Pathology and Adaptation, 2022.
[21] L. Liu, X. Ma, L. Yan, and Y. Wang, "An innovative reinforcement method: the combination of CFRP bars and UHPC layer is applied to the flexural reinforcement of RC beams," Multidiscipline Modeling in Materials and Structures, vol. 18, no. 2, pp. 308–327, 2022.

[22] Chinese National Standards, Code for Design of Steel Structures GB 50017-2003, Chinese Standard Press, Beijing, 2003. [33] J. G. Nie and Y. H. Wang, "Comparison study of constitutive model of concrete in ABAQUS for static analysis of structures," Engineering Mechanics, vol. 30, no. 4, pp. 59–67, 2013.
[23] J. G. Nie and Y. H. Wang, "Comparison study of constitutive model of concrete in ABAQUS for static analysis of structures," Engineering Mechanics, vol. 30, no. 4, pp. 59–67, 2013.
[24] S. H. Lee, A. Abolmaali, K. J. Shin, and H. D. Lee, "ABAQUS modeling for post-tensioned reinforced concrete beams," Journal of Building Engineering, vol. 30, Article ID 101273, 2020.
[25] ABAQUS, ABAQUS Analysis User's Manual Version 6.13, Assault Systems, Dassault Systems Simulia Corporation, Rhode Island, USA, 2013.
[26] A. Raza, Q. U. Z. Khan, and A. Ahmad, "Numerical investigation of load-carrying capacity of GFRP-reinforced rectangular concrete members using CDP model in ABAQUS," Advances in Civil Engineering, vol. 2019, pp. 1745341– 1745421, 2019.
[27] Chinese National Standards, Code for Design of Concrete Structures GB 50010-2010, China Building Industry Press, Beijing, 2015.
[28] Z. Zhang, X. D. Shao, W. G. Li, P. Zhu, and H. Chen, "Axial tensile behavior test of ultra high-performance concrete," China Journal of Highway and Transport, vol. 28, no. 8, pp. 50–58, 2015.
[29] P. R. Prem, A. Ramachandra Murthy, and B. H. Bharatkumar, "Influence of curing regime and steel fibers on the mechanical properties of UHPC," Magazine of Concrete Research, vol. 67, no. 18, pp. 988–1002, 2015.
[30] American Association of State Highway and Transportation Ofcials, Load and Resistance Factor Design (AASHTO. LRFD) (2017), Bridge Design Specifcations, 8th Ed edition.
[31] American Concrete Institute (ACI), Building code requirements for structural concrete and commentary, ACI 318R–11, Farmington Hills, MI, USA, 2011.
[32] K. Park, H. Choi, and G. H. Paulino, "Assessment of cohesive traction-separation relationships in ABAQUS: a comparative study," Mechanics Research Communications, vol. 78, pp. 71–78, 2016.
[33] D. W. Spring and G. H. Paulino, "A growing library of three-dimensional cohesive elements for use in ABAQUS," Engineering Fracture Mechanics, vol. 126, pp. 190–216, 2014.
[34] P. Feng, H. L. Qing, and L. P. Ye, "Discussion and definition on yield points of materials, members and structures," Engineering Mechanics, vol. 34, no. 3, pp. 36–46, 2017.